DEPARTMENT OF MECHANICAL & AEROSPACE ENGINEERING

University of Strathclyde Engineering

Class Code/ Title:	ME409: Individual Project
Technical paper title:	An investigation of the feasibility of using electric propulsion as a means of deorbiting end of life satellites in middle and geostationary orbits (MEO) (GEO).
Student Name/ Number:	201607942
Supervisor:	Dr S. Grey
Date:	25/03/2020
Word count:	2998

Abstract

This work investigated the use of electric propulsion as a space-debris mitigation technique for higher altitude satellites. The proposed solutions had to adhere to current industry regulations while reducing the risk of further collisions in orbit. A numerical model of a two-body orbit was devised in Python 3.7 to simulate the thrust, J2-effect and aerodynamic-drag acting on the spacecraft, several qualified thrusters were simulated across a series of orbital altitudes. Thrusters were evaluated in terms of power, mass, cost and manoeuvre times. The results indicated two candidates that could manoeuvre a 2000kg satellite from GEO to a deorbit altitude of 200km; one offered shorter manoeuvre times with reduced power requirements, however, the other offered a significant reduction in propellant mass at the expense of higher power. Utilising electric propulsion over chemical propulsion yielded an average 94.2% propellent saving which translated to an estimated $30-65M USD saving from launch.

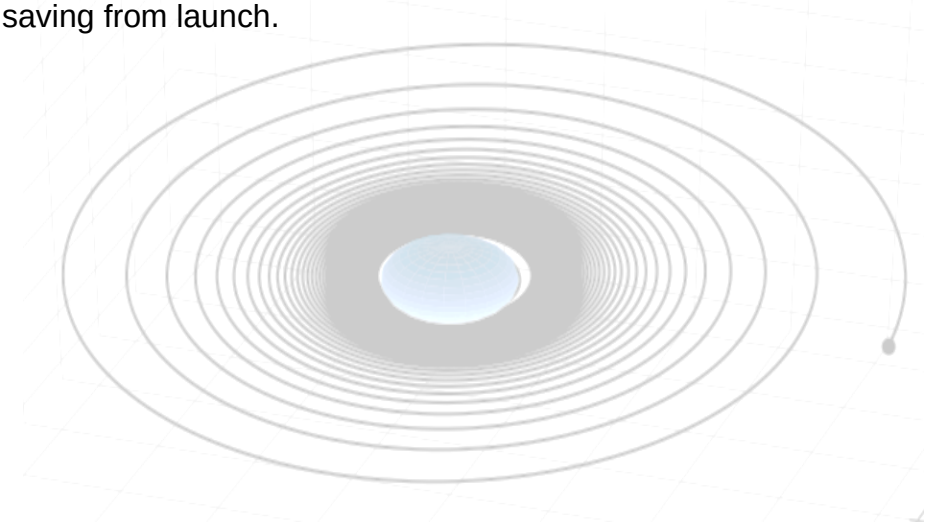

Contents

Nomenclature

Symbol	Description	Units
A	Satellite area	m^2
$\|ATM\|$	Atmospheric direction vector	ms^{-1}
a_{j2}	J2 component of acceleration	ms^{-2}
a_{thrust}	Acceleration component due to thruster	ms^{-2}
C_d	Coefficient of drag	-
e	Orbital eccentricity	-
E_m	Energy required for manoeuvre	GJ
F_t	Total Thrust Force	N
g_0	Gravitational Constant for earth	ms^{-2}
h	Angular momentum vector	m^2s^{-1}
H_i	Scale height	m
i	Orbital Inclination	rad
I_{sp}	Specific Impulse	Sec
M	Mean molecular molar mass	$kg.mol^{-1}$
m_1	Mass of earth	kg
m_2	Mass of satellite	Kg
m_{prop}	Mass of propellant required for manoeuvre	kg
m_{ppu}	Mass of required power conditioning units	kg
n	Nodal line	m
N	Ratio of initial & final radii	-
R	Gas Constant	-
$\overrightarrow{r_1}$	Radial vector of earth	m
$\overrightarrow{r_2}$	Radial vector, earth to satellite	m
T	Mean atmospheric temperature	K
t_m	Time taken to deorbit	seconds
V	Magnitude of satellite velocity	ms^{-1}
v_{normed}	Velocity unit vector	-
$V_{\frac{sc}{atm}}$	Spacecraft velocity relative to atmosphere	ms^{-1}
z	Altitude	m
V	Magnitude of satellite velocity	ms^{-1}
α	Semi-major axis	m
Δv	Change in Velocity	ms^{-1}
ΔV_H	Hohmann Transfer – change in velocity	ms^{-1}
ΔV	Perturbation Theory – change in velocity for EP	ms^{-1}
μ	Standard gravitational parameter	m^3s^{-2}
υ	True anomaly	rad
ρ	Air density	kgm^{-3}
ρ_{SL}	Air density at sea-level	kgm^{-3}
$\rho(z)$	Air density as a function of altitude	kgm^{-3}
Ω	Rising ascending node	m
ω	Argument of periapsis	rad

1.0 Introduction

1.1 Scope

The aim of this work was to investigate the feasibility of using electric propulsion (EP) for deorbiting end of life satellites. Several thrusters were simulated across multiple altitudes to investigate the suitability of the thrusters in terms of power, mass, cost and manoeuvre times. Four thrusters were selected, and system architecture was discussed alongside a cost-comparison of chemical propulsion (CP) thrusters to assess the cost benefit of the transition.

It has become evident that space-debris is a serious issue facing the space-industry - if not suitably addressed, current models indicate there is a significant risk of setting off a chain reaction known as the Kessler Syndrome [1]**.** The reaction would cause an exponential increase in the creation of new debris through a higher object collision rate, which would elevate the risk above a safe level for space-operations. This study investigated EP as a new space-debris mitigation strategy which would, when implemented, reduce the risk of further collisions. Furthermore, it was imperative that solutions adhered to ESA /NASA spaceflight guidelines specified below [2] [3].

1. *"The final orbit shall grant a decay time of less than 25 years…"*
2. *"The final orbit must pose no risk to human space flights..."*
3. *"The final orbit shall allow the debris to leave the region within 1 year."*

2.0 Literature Review

2.1 Propulsion in Space

In space, there are two methods of producing thrust. The first and most commonly employed method is CP, which produces thrust through a combustion process, occurring typically in a high-pressure reaction chamber where hot gas is accelerated through a nozzle to provide thrust [4]**.**

Conversely, EP is a hypernym for a range of systems that exploit the interaction between an electromagnetic field and charged particles. The interaction is facilitated by the ionisation and acceleration of propellant gas to produce thrust. Although EP systems tend to operate on the same underlying principle, they can be categorised into three groups by how they accelerate particles: Electrothermal, Electrostatic and Electromagnetic [5].

Analysis of the physical phenomena defined above had limited value to the technical study and is out-with the scope of this report. However, an in-depth explanation of their physical characteristics can be found in the literature [5] [6].

The advantages of EP were deduced from table-1 and equation-1, specific impulse I_{sp} was calculated by dividing thrust-force F_t, by a rocket's mass-flow rate $\dot{m}$, multiplied by the gravitational constant g_0. Hence, I_{sp} can be defined as the power to thrust ratio of a propulsion system. EP systems' higher I_{sp} ranges yield improvements to payload-mass fractions, due to lower $\dot{m}$ but operate at lower F_t ranges [6].

$$I_{sp} = \frac{F_{thrust}}{\dot{m} g_0} \quad Eqn.2$$

Table 1 – CP and EP thruster performance ranges [5].

Thruster Type	Specific Impulse (sec)	Thrust Range (mN)	Input Power (kW)	Efficiency (%)	Typical Propellant Utilisation
Cold Gas	50-75	500-60000	-	-	Various
Chemical (monopropellant)	150-225	30-80000	-	-	N_2H_4 H_2O_2
Chemical (Bipropellant)	300-450	30-100000	-	-	Various
Resistojet	300-325	200-300	0.5-1.1	65-90	N_2H_4
Arcjet	500-600	200-1000	0.9-2.2	25-45	N_2H_4
Ion Thruster	1500-4900	0.01-500	0.4-4.3	40-80	Xenon
Hall Thruster	900-2600	0.01-2000	1.5-4.5	35-60	Xenon
PPT's	850-1200	0.05-10	<0.2	7.5-13	Teflon

Table-1 shows that EP is power-intensive compared to CP. The limitations of power generation in space are often the deciding factor in selecting propulsion systems [7]. However, the combined effect of improved solar-arrays, advanced lithium-ion batteries, and sophisticated power-conditioning units led to an increase in spacecraft power-capacity [8]. It was key to identify a nominal power input range to scope thrusters, to compensate for efficiencies and degradation of power systems across a mission life of 10-15 years. After which, designers must assess the spacecraft's power integrity, in order to provide constant power to the thrusters throughout its final manoeuvre. Figure-1 identifies EP systems' regions of mission utility for various thrusters.

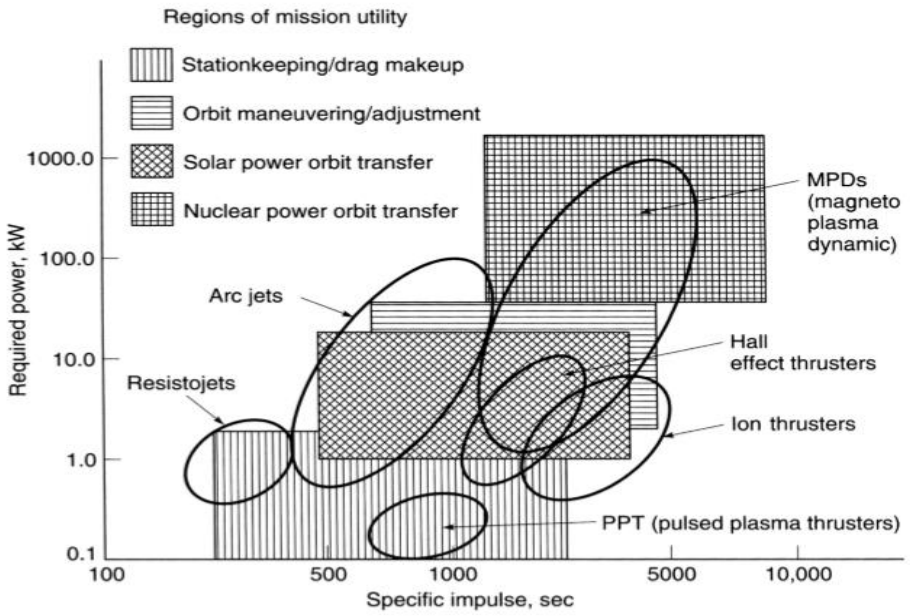

Figure 1 - Regions of mission utility for EP systems [7].

Ion and Hall-effect thrusters (HET) were selected due to their relatively low power range P_{in}, of 0.5-10kW and large I_{sp}, ranges of 1000-5000. Moreover, this assertion was supported by a host of successful missions such as; GOCE, SMART-1, Hayabusa, Deepspace-1 and Dawn [9] [10] [11].

2.2 Post Mission Disposal Manoeuvre (PMD)

The strategy for PMD with CP systems would be modelled on a reversed Hohmann transfer. The method detailed in figure-2 entails scheduled retrograde burns to decrease the apogee velocity until the final circularised orbit has been reached [12]. The final position tends to be within very low earth orbits to allow the atmospheric drag to rapidly decelerate and heat the craft to burn up prior to re-entry.

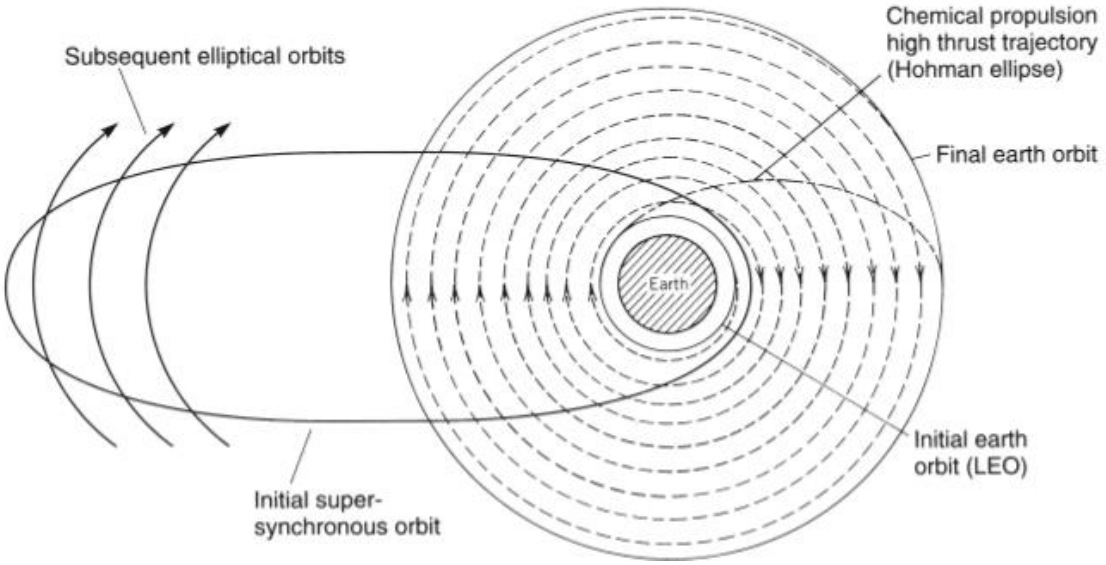

Figure 2 - Proposed CP & EP manoeuvre trajectories detailing a Hohmann transfer and a gradual spiral towards target orbit. [7].

Figure-2 details the desired trajectory for an EP PMD mission, the spiral descent [7] [13]. Unlike Hohmann transfers, spiral manoeuvres are constant thrust and non-Keplerian and are only solvable through numerical integration where time becomes a key parameter. It was noted that the ΔV, for a spiral manoeuvre would be greater than the equivalent Hohmann transfer, but it was considered useful to compare each.

3.0 Method

The below programme was built using Python 3.7 with NumPy, SciPy and Matplotlib [14] [15]. The source code is available in appendix[7.1] and GitHub. The methodology outlined below details the underlying mathematics used to construct the model.

3.1 Deriving the System: Two body Mechanics

Section 3.1 details key components of building a steady state two-body mechanics problem.

3.1.1 Newton's Law of Gravitation

It was pertinent to the body of work to first understand the underlying physics of two-body orbit problems between a spacecraft and earth. Both objects were treated as point-masses, and in the absence of external forces, the equation of motion for the masses were stated as equation-2-3 [16].

$$m_1 \frac{d^2\overrightarrow{r_1}}{dt^2} = Gm_1m_2 \frac{\vec{r}_2 - \vec{r}_1}{|\vec{r}_2 - \vec{r}_1|.^3} \qquad Eqn.2$$

$$m_2 \frac{d^2\overrightarrow{r_1}}{dt^2} = -Gm_1m_2 \frac{\vec{r}_2 - \vec{r}_1}{|\vec{r}_2 - \vec{r}_1|.^3} \qquad Eqn.3$$

The position vector was defined as $\vec{r}_2 - \vec{r}_1 = \vec{r}$, and hence equation-3 was subtracted from equation-2 and yielded a single equation of motion below, equation-4.

$$\frac{d\vec{v}}{dt} + \mu \frac{\vec{r}}{r^3} = 0 \qquad Eqn.4$$

Where $v = \frac{dr}{dt}$ and $\mu = G(m_1+m_2)$. The mass of the satellite m_1 is negligible with respect to the mass of the earth m_2, therefore $\mu = Gm_1$. Newton's law-of-gravitation was directly integrated, yielding an acceleration vector a = [a_x, a_y, a_z]. Equation-4 was defined in the function `ODE` within the `orbit_propagator_script`. [17]

3.1.2 Implementation of numerical integrator

The integrator `LSODA` was selected from the SciPy package to numerically evaluate equation-4. `LSODA` utilised the Adam-Bashford multistep method, which produced highly accurate results and reduced computational cost when compared to lower order schemes [18].

3.1.3 State Vector to Classical Orbital Elements (COES)

The programme required a conversion algorithm with an input of cartesian state-vectors to COES, to accurately define the manoeuvre in all six degrees of freedom [19] [20]. COES were defined as inclination, eccentricity, rising-ascending node, argument of periapsis, true anomaly and semi-major axis.

The angular momentum vector denoted *h* was required for calculating inclination, eccentricity and node-line, it was computed by taking the cross product of position and velocity vectors in equation-5. The orbital inclination *i*, was calculated in equation-6 by dividing h_z by the magnitude of the angular momentum vector.

$$h = r \times \dot{r} \quad \left[\frac{m^2}{s}\right] \qquad Eqn.5$$

$$i = arccos\frac{h_z}{\|h\|} \qquad Eqn.6$$

Next, the eccentricity vector was calculated from equation-7 where $\mu = \mu_{earth} = 6.67408E\text{-}11$. Now, as per equation-8 the node-line was computed.

$$e = \frac{h \times \dot{r}}{\mu} - \frac{r}{\|r\|} \qquad Eqn.7$$

$$n = (0 \quad 0 \quad 1)^T \times h = (-h_y \quad h_x \quad 0)^T \qquad Eqn.8$$

The longitude of the rising ascending node Ω, was calculated using equation-9 with applied conditional statements, regarding the input of the node-line vector.

$$if;\ n_y \geq 0, \qquad \Omega = arccos\frac{n_z}{\|n\|} \qquad Eqn.9$$

$$else;\ n_y < 0, \qquad \Omega = 2\pi - arccos\frac{n_z}{\|n\|}$$

Similarly, in equation-10, conditional statements are imposed on the input of eccentricity to calculate the argument of periapsis.

$$if;\ e_z \geq 0, \qquad \omega = arccos\frac{\langle n, e\rangle}{\|n\|\|e\|} \qquad Eqn.10$$

$$else;\ e_z < 0, \qquad \omega = 2\pi - arccos\frac{\langle n, e\rangle}{\|n\|\|e\|}$$

The required eccentricity is derived from the normalised magnitude of the eccentricity vector, and henceforth, mathematically $e = \|e\|$.

Normalised eccentricity was used to calculate true anomaly υ.

$$if;\ r, \dot{r} \geq 0, \qquad \upsilon = arccos\frac{\langle e, r\rangle}{\|e\|\|r\|} \qquad Eqn.11$$

$$else; \qquad \upsilon = 2\pi - arccos\frac{\langle e, r\rangle}{\|e\|\|r\|}$$

Finally, the semi-major axis, α was calculated as per equation-12.

$$\alpha = \frac{1}{\frac{2}{\|r\|} - \frac{||\dot{r}||^2}{\mu}} \qquad Eqn.12$$

3.2 Implementation of Orbital Perturbations

Perturbations considered were subsequently defined in *sections 3.2.1, 3.2.2 and 3.3.3* – their characteristics were specified within the function; `null_perts()` which returned a dictionary. This allowed the use of Boolean-logic to turn perturbations on and off while building and testing the model.

3.2.1 J2 Effect

The J2-effect [21], or earth's oblateness, is the strongest perturbation of all the non-spherical J-terms, therefore it was practical to consider its effects. The J2-effect was introduced into the model by the addition of the a_{J2}, into equation-13, and was rearranged for acceleration in equation-14, Newton's law-of-gravitation.

$$\frac{d\vec{v}}{dt} + \mu \frac{\vec{r}}{r^3} + a_{J2} = 0 \quad Eqn.13$$

$$\therefore a_{xyz} = \mu \frac{\vec{r}}{r^3} + a_{J2} \quad Eqn.14$$

a_{J2} was calculated with perturbation theory by partially differentiating v_{J2} with respect to the spatial directions to generate expressions for acceleration in equation-15 [22].

$$a_x = -\frac{\mu\vec{x}}{r^3}\left\{1 + \frac{3}{2}J_2\left(\frac{r}{r}\right)^2\left(1 - \frac{5z^2}{r^2}\right)\right\}$$

$$a_y = -\frac{\mu\vec{y}}{r^3}\left\{1 + \frac{3}{2}J_2\left(\frac{r}{r}\right)^2\left(1 - \frac{5z^2}{r^2}\right)\right\} \quad Eqn.15$$

$$a_z = -\frac{\mu\vec{z}}{r^3}\left\{1 + \frac{3}{2}J_2\left(\frac{r}{r}\right)^2\left(3 - \frac{5z^2}{r^2}\right)\right\}$$

The components of equation-15 were passed as an array into equation-14 and were simply added to the acceleration vector.

3.2.2 Aerodynamic Drag

Aerodynamic drag is considered to have a substantial effect in satellites within lower earth orbit. Equation-16 magnitude is dependent on a craft's effective area A, velocity magnitude V, variable density value of ρ and a coefficient of drag C_d - which was assumed to be 2.2 [23] [24]**.**

$$F_d = -C_d.A.\rho.\frac{V^2}{2} \quad Eqn.16$$

The U.S. Standard Atmosphere model 1976 [25] was applied to model variations in atmospheric density at approximately; 60.096km, 251.189km and 1000km, the vector quantity was stored within the `planetary_data_file`. The first step of the algorithm, equation-17, was to calculate altitude:

$$z = |\vec{r_2}| - |\vec{r_1}| \quad Eqn.17$$

The algorithm required computation of air density at satellites current altitude. It was assumed that the effects of the atmosphere were negligible above 1000km and hence ρ = 0. Therefore, density as a function of altitude can be calculated as equation-18 [26]:

$$\rho(z) = \rho_{SL} \cdot e^{-\frac{z}{H_i}} \qquad Eqn.18$$

Where ρ_{SL} was defined as air density at sea level and H_i was defined as altitude increment where the density decreases by a factor of $e^{-1} \approx 0.4$ which can be derived from gas-law relation observed in equation-19;

$$H_i = \frac{RT}{Mg} \qquad Eqn.19$$

Moreover, the atmosphere is not fixed within the earth centred inertial frame and instead rotates with the earth. Equation-20 was used to calculate the motion of the spacecraft relative to the atmosphere by using spacecraft velocity in the earth centred inertial frame and subtracting the cross-product of the atmospheric velocity vector $|ATM|$, and the spacecraft's position vector.

$$V_{sc/atm} = V - |ATM| \cdot |R| \qquad Eqn.20$$

The atmosphere vector was calculated as per equation-21 by taking one full revolution of earth and dividing it by the hours in one day [27].

$$|ATM| = \frac{2\pi}{86160\ (23\ hours\ 56\ minute)} = |ATM|\ \hat{z} \qquad Eqn.21$$

The above values were substituted into equation-22 and divided by the satellite mass and added to the acceleration vector.

$$a_d = -\frac{C_d . A . \rho(z) V_{sc/atm}}{m_{sat}} \qquad Eqn.22$$

3.2.3 Thrust

Acceleration provided by EP modules could be calculated using Newton's 2nd law:

$$F_{thrust} = m_{sat} \cdot a_{thrust} \quad Eqn.23$$

The thrust vector was given direction by taking the velocity vector V and dividing it by the normalised vector quantity, yielding the unit vector [26]. The parameter was assigned a thrust direction integer of -1 to indicate that the thrust vector must act against the velocity vector, and act as a deorbit manoeuvre.

$$v_{normed} = \frac{[v]}{|v|} \quad Eqn.24$$

Equation-23 and equation-24 were multiplied together and rearranged to yield equation-25:

$$a_{thrust} = -\left(\frac{[v]}{|v|}\right) \frac{F_{thrust}}{m_{sat}} \quad Eqn.25$$

All perturbations were then substituted into Newton's law-of-gravitation which gives the full equation of motion in equation-26.

$$a = \mu \frac{\vec{r}}{r^3} + a_{J2} + a_{drag} + a_{thrust} \quad Eq.26$$

3.3 Mission Parameters

3.3.1 Thruster Selection

Table 2 - EP Specifications for thrusters simulated [7] [28].

Thruster	Power (W)	Impulse (sec)	Thrust (mN)	Efficiency (%)	Mass (kg)	Max-Burn (hr)
SPT100D	2500	2200	112	52	4.7	11680
XIPS-25	4250	3550	165	67	13.7	13370
PPS1350	1400	1660	90	55	5.3	9500
BPT 4000	4500	1950	270	59	7.5	8000

Table-2 shows the selected thruster systems, it comprises of both Ion & HET systems and represent a broad range of power, I_{sp} and thrust. Their selection was based on the proven operational history in spaceflight and their use is limited by their respective mass burn time.

3.3.2 Orbit Selection

Manoeuvres were simulated at altitudes of 7825km, 19100km, 23222km and 35786km using the devised 2000kg satellite 'SAT-1' – Appendix[7.2] - to assess various thrusters. Two-line element files were extracted from CelesTrak-API [29] in order to generate accurate satellite input data.

3.3.3 Stop Conditions

The study assumed constant power and did not account for an eclipse period. Thus, continuous thrust was applied from the satellite's initial position until 200km altitude was reached. The final altitude was considered sufficiently deorbited, due to the prominence of atmospheric-drag at that altitude [30] With stop conditions defined, total change in velocity ΔV was calculated as equation-27:

$$\Delta V \approx \sqrt{\frac{\mu}{r_0}} - \sqrt{\frac{\mu}{r}} \qquad Eqn.27$$

The Hohmann transfer detailed in *Section-2.2* was given as equation-28.

$$\Delta V_H = \left(\sqrt{\frac{2\mu r}{r_0(r+r_0)}} - \sqrt{\frac{\mu}{r_0}}\right) + \left(\sqrt{\frac{\mu}{r}} - \sqrt{\frac{2\mu r_0}{r(r+r_0)}}\right) \qquad Eqn.28$$

Hence, by assuming radii r and r_0 are related by $r = Nr_0$ where N is the number of revolutions, the ratio of divergence from Hohmann transfer was calculated as equation-29:

$$\frac{\Delta V}{\Delta V_H} = \left[\sqrt{2\left(1 + \frac{2\sqrt{n}}{n+1}\right)} - 1\right]^{-1} \qquad Eqn.29$$

4.0 Results

Section 4.1 details simulation results for deorbit manoeuvres across various altitudes with thrusters specified in *section 3.3.1.*

4.1 Simulation Outputs

Figure-3 shows manoeuvre times from 7825km with selected thrusters with additional data in table-3. BPT4000 produced the lowest manoeuvre-time (t_m) of 4319 hours. PPS1350 took 13045 hours, which disqualified its use, as t_m is out-with the thruster's maximum burn-time of 9500 hours. Disqualified thrusters have been highlighted red and suitable thrusters green in tables-3-6.

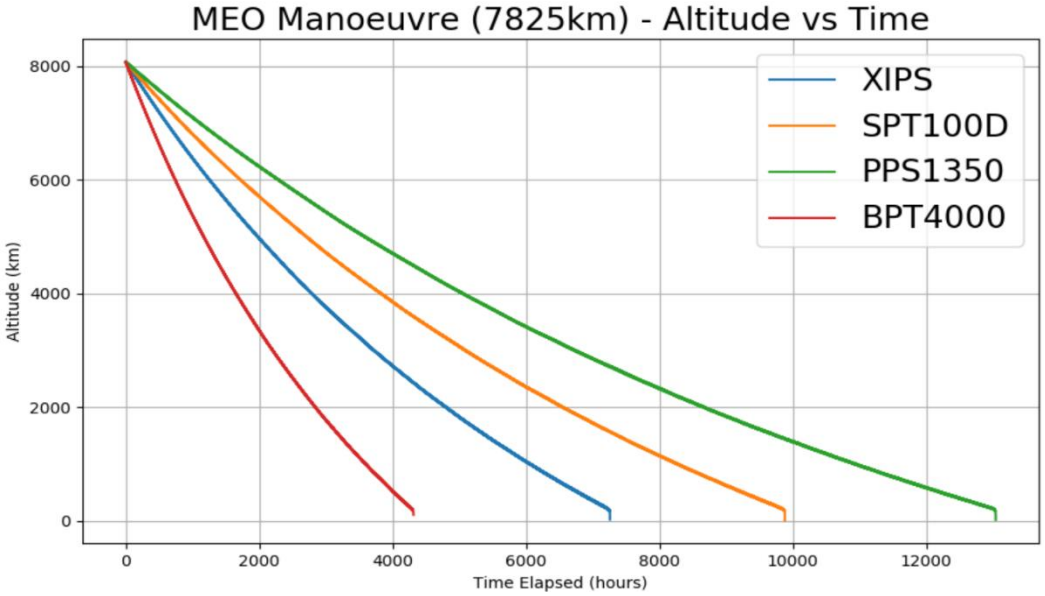

Figure 3 – Simulated manoeuvre from 7825km to 200km with EP systems

Figure-4 and table-4 show results from 19100km, SPT100D was disqualified from use, due to a t_m of 14975 hours with a maximum burn time of 11680 hours.

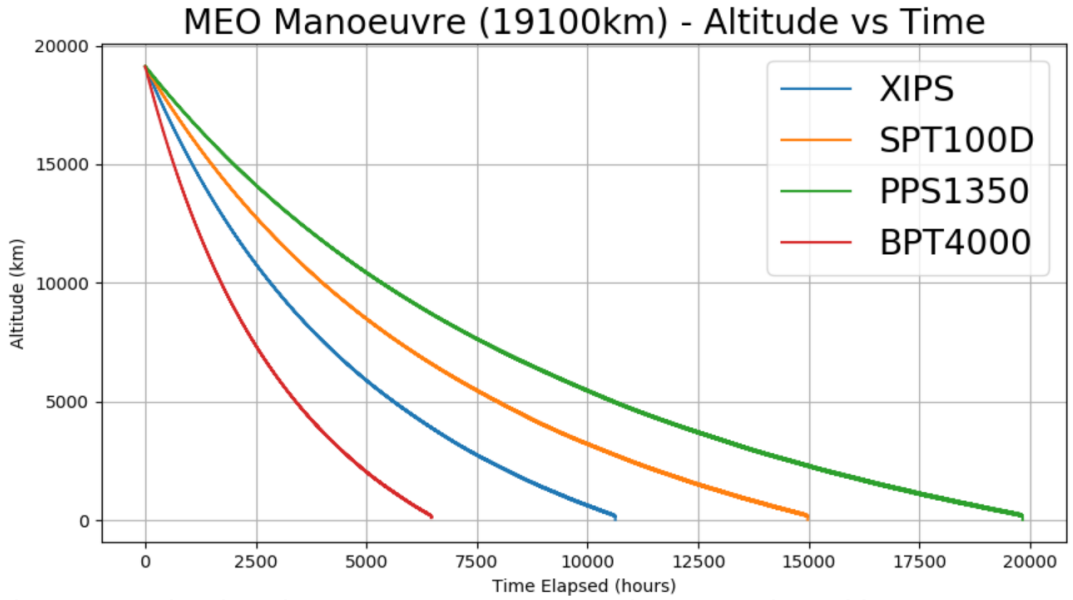

Figure 4 – Simulated Manoeuvre from 19100km to 200km with EP systems.

Table 3 - Results from PMD at 7825km with EP systems, where t_m denoted time, E_m denoted energy used and M denotes mass.

Manoeuvre from 7825km									
	tm **(second)**	***Mprop*** **(kg)**	***Mppu*** **(kg)**	***tm*** **(hour)**	***tm*** **(days)**	***Em*** **(GJ)**	***Mtotal*** **(kg)**	$\frac{\Delta V}{\Delta VH}$	**Max Burn Time (Hour)**
SPT100D	35581350	184.65	20.83	9883.71	411.82	89	2710.18	1.614	11680
XIPS	26140350	123.85	21.57	7261.21	302.55	111	2659.12	1.614	13370
PPS1350	46962750	259.55	14.14	13045.21	543.55	65.7	2778.99	1.614	9500
BPT 4000	15549750	213.99	24.19	4319.38	179.97	70	2745.68	1.614	8000

Table 4 – Results from PMD at 19100km with EP systems, where t_m denoted time, E_m denoted energy used and M denotes mass.

Manoeuvre from 19100km									
	t_m **(second)**	M_{prop} **(kg)**	M_{ppu} **(kg)**	t_m **(hour)**	t_m **(days)**	E_m **(GJ)**	M_{total} **(kg)**	$\frac{\Delta V}{\Delta V_H}$	**Max Burn (Hour)**
SPT100D	53911200	279.77	31.25	14975.33	623.97	135	2815.72	1.815	11680
XIPS	38260500	181.27	32.36	10627.92	442.83	163	2727.34	1.815	13370
PPS1350	71408700	394.65	21.21	19835.75	826.49	100	2921.17	1.815	9500
BPT 4000	23305050	320.71	36.29	6473.63	269.73	105	2864.50	1.815	8000

Figure-5 details the manoeuvre from 23222km, due to the weakened gravity field and the relatively small distance, similar results were recorded between 19100km and 23222km – see table-4-5.

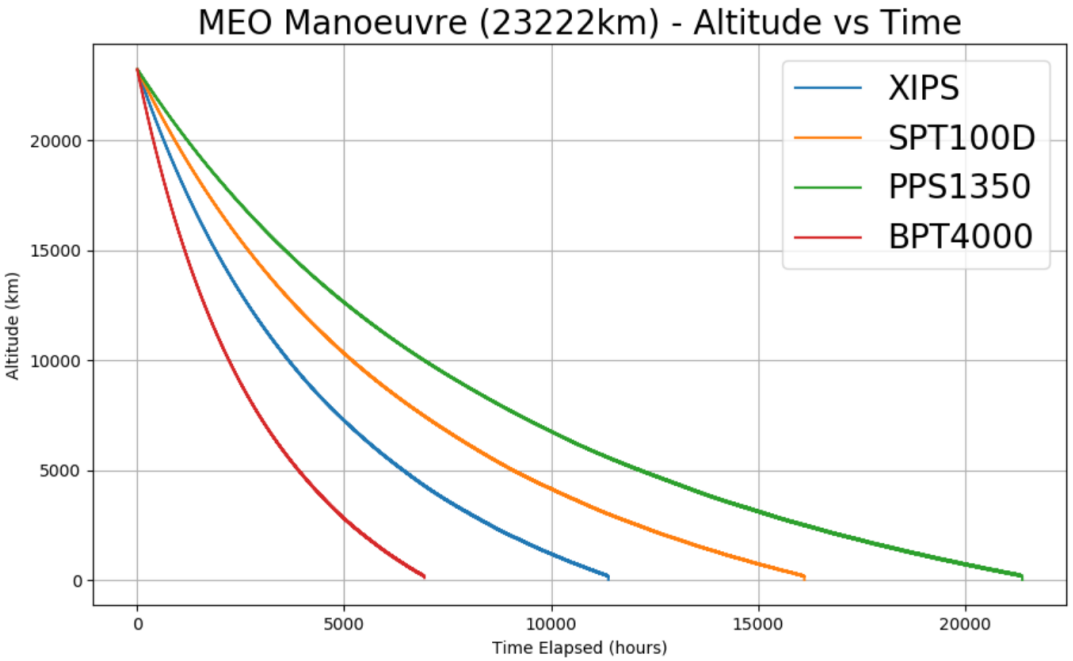

Figure 5 – Simulated manoeuvre from 23222km to 200km with EP systems.

Figure-6 highlights two appropriate thrusters for satellites in geostationary orbits. XIPS-25 and BPT4000 have a suitable range for a 2000kg satellite, XIPS-25 greater I_{sp}, yielded a 181kg propellant saving over BPT4000 but takes a further 4270 hours to complete the manoeuvre. Additional COES data for successful manoeuvres can be viewed in Appendix[7.3]

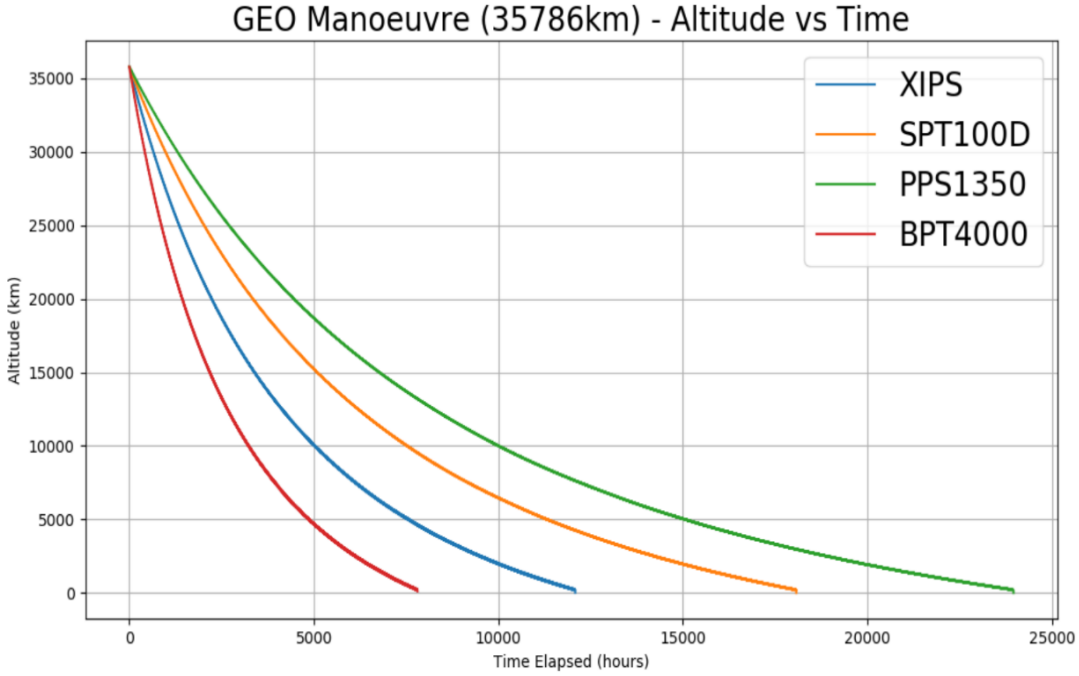

Figure 6 – Simulated manoeuvre from 35786km to 200km with EP systems.

Table 5 - Results from PMD at 23222km with EP systems, where t_m denoted time, E_m denoted energy used and M denotes mass.

Manoeuvre from 23222km									
	t_m (second)	M_{prop} (kg)	M_{ppu} (kg)	t_m (hour)	t_m (days)	E_m (GJ)	M_{total} (kg)	$\frac{\Delta V}{\Delta V_H}$	Max Burn (Hour)
SPT100D	58027800	301.14	41.67	16118.83	671.62	135	2847.50	1.856	11680
XIPS	40985400	194.19	43.15	11384.83	474.37	163	2751.03	1.856	13370
PPS1350	76990650	425.50	28.28	21386.29	891.10	100	2959.09	1.856	9500
BPT 4000	24946800	343.30	48.39	6929.67	288.74	105	2899.19	1.856	8000

Table 6 - Results from PMD at 35786km with EP systems, where t_m denoted time, E_m denoted energy used and M denotes mass.

Manoeuvre from 35786km									
	t_m (second)	M_{prop} (kg)	M_{ppu} (kg)	t_m (hour)	t_m (days)	E_m (GJ)	M_{total} (kg)	$\frac{\Delta V}{\Delta V_H}$	Max Burn (Hour)
SPT100D	65050650	337.58	52.08	18069.63	752.90	163	2894.36	1.94	11680
XIPS	43494300	206.07	53.93	12081.75	503.41	185	2773.71	1.94	13370
PPS1350	86241300	476.63	35.35	23955.92	998.16	121	3017.28	1.94	9500
BPT 4000	28122600	387.01	60.48	7811.83	325.49	127	2954.99	1.94	8000

Performance plots were generated for BPT4000 and XIPS-25 thrusters at geostationary orbits. Figure-7-8 shows BPT4000 and XIPS-25, altitude against t_m plots, were mass was incrementally increased by 200kg up to 6000kg. Thrusters t_m increased on average by 35.68 and 57.6 days per increment for BPT4000 and XIPS-25 respectively.

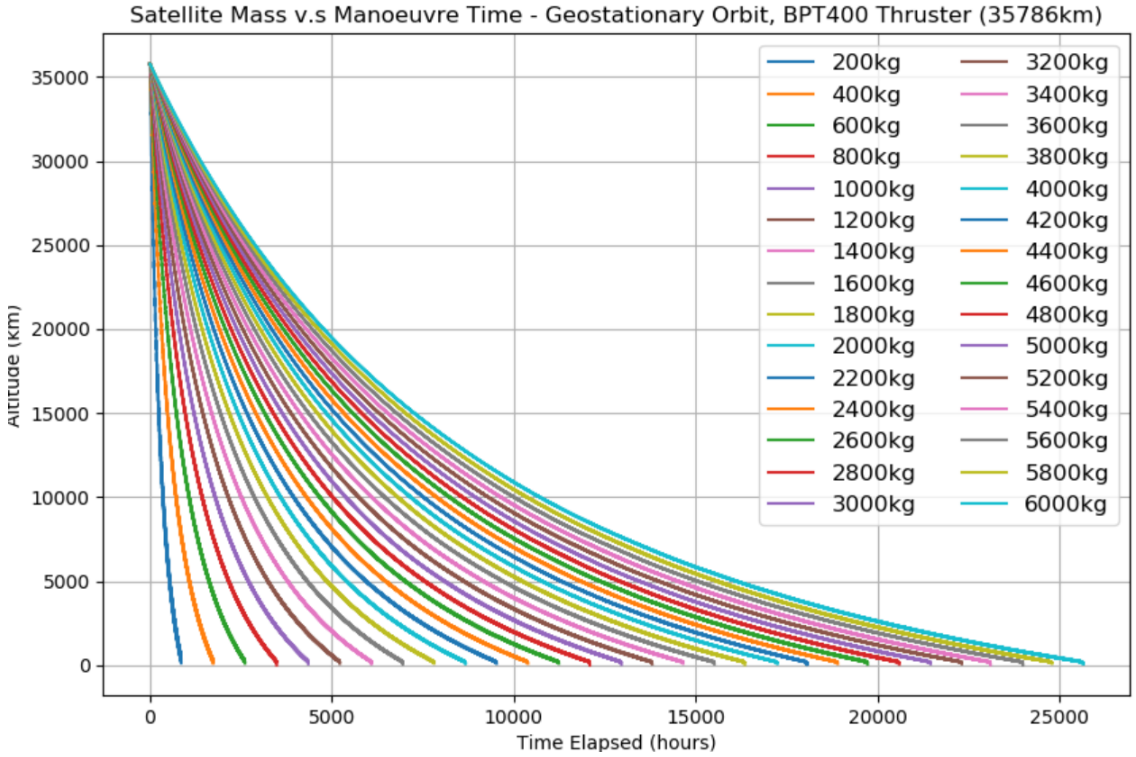

Figure 7 – Performance curve, showing how mass affects deorbit times

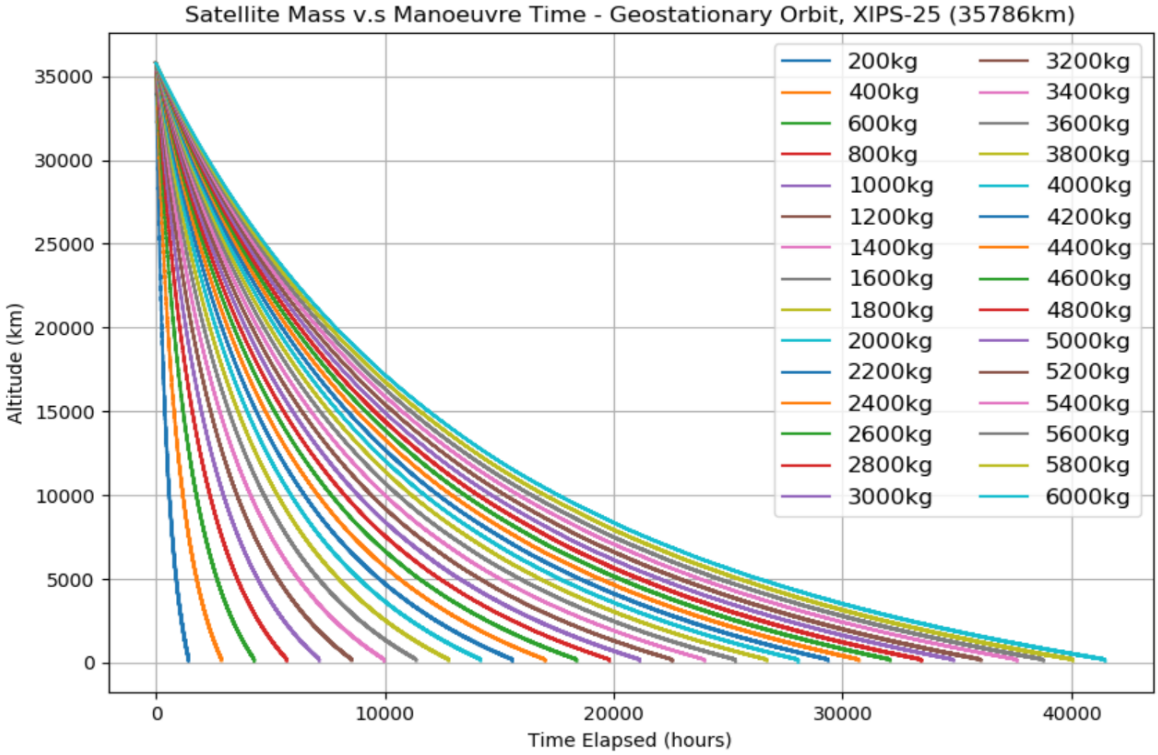

Figure 8 – Mass vs. time performance curve (GEO, XIPS-25)

4.2 Model Validation

The model was validated in order to confirm accuracy of results. Initial velocities were calculated analytically, and the model results, detailed in table-7, were printed to the console.

Table 7 – Model validation with initial velocity.

Velocity at Initial Altitude Verification					
Analytical Solution		**Model Solution**		**Calculated Error**	
Altitude (km)	***Speed (km/s)***	***Altitude (km)***	***Speed (km/s)***	***ABS Error (km/s)***	***REL Error (%)***
7825	5.29780	7825	5.29759	0.00021	0.0040
19100	3.95539	19100	3.95535	0.00036	0.00092
23222	3.66964	23222	3.66963	0.00016	0.00037
35786	3.07464	35786	3.07466	-0.00019	0.00063

The calculated absolute and relative errors shown in table-7 indicated less than 0.01% error in all recorded instances for initial velocity. The model was built and tested across the range of altitudes, mission ΔV was noted and was calculated analytically for the comparison below, table-8.

Table 8 – Model validation with total mission ΔV's

Mission ΔV Verification					
Analytical Solution		**Model Solution**		**Calculated Error**	
Altitude (km)	***Mission ΔV (km/s)***	***Altitude (km)***	***Mission ΔV (km/s)***	***ABS Error (km/s)***	***REL Error (%)***
7825	2.4874	7825	2.4867	0.00073	0.029
19100	3.8298	19100	3.8289	0.00091	0.023
23222	4.1156	23222	4.1147	0.00093	0.022
35786	4.7106	35786	4.7096	0.00096	0.020

Mission ΔV errors between the analytical and model in the absence of perturbations, yielded an approximate relative error of 0.0242%.

5.0 Discussion

5.1 Model Limitations

Errors outlined in *Section-4.2* indicated that results gained are highly accurate and, in all instances, yield below 0.01% relative error between analytical and model solutions. However, there were inherent limitations with the model that were abstract and more difficult to quantify – e.g. utilising velocity thrust vectoring, which although appropriate for this estimation, is not the optimal method of transfer. Furthermore, the range of perturbations modelled were limited to the J2 effect and aerodynamic-drag, as they exert the most noticeable perturbation-effects on the satellite. However, given the length of such manoeuvres, there exists a host of J parameters where, in the interest of greater precision, it would be prudent to model [31]. Further simulations could be undertaken to account for eclipse periods, more J parameters, the moon's gravity alongside the implementation of solar-radiation pressure effects. One limitation of deorbiting in this manner would be the manoeuvring of a satellite through debris-dense zones with reduced attitude control capacity, which, may in turn contribute to the problem.

5.2 Thruster Evaluation

The PPS1350 was unsuitable for the range of required manoeuvres. At 7825km, three thrusters (table-3) could perform the manoeuvre, as their maximum burn-time exceeded the t_m. However, at higher altitudes (table-4-6) SPT100D exceeded its burn-time, hence BPT4000 and XIPS-25 were the only thrusters capable of performing the manoeuvre across all altitudes. BPT4000 can supply 41.07% more thrust and is suitable for manoeuvring heavier satellites but requires 170kg more fuel than XIPS-25 to perform a GEO manoeuvre for a 2000kg satellite, conversely, XIPS-25 improved fuel efficiency comes at the expense of greater energy requirements and increased t_m.

This study only simulated single thrusters in operation but in many instances multiple thrusters are clustered together to increase thrust [32]. Clustered configurations were not considered in this work, but their advantages were noted, for comparison the PPS1350 was arranged in a two-thruster arrangement and compared to the XIP-25.

Table 9 - XIPS-25 with PPS1350 (x2) to highlight the effect of clustering.

Thruster Types	Power (W)	Impulse (sec)	Thrust (mN)	Efficiency (%)	Mass (kg)	Run-Time (hr)
XIPS-25 (x1)	4250	3550	165	67	13.7	13370
PPS1350 (x2)	2800	1660	180	55	10.6	9500

Table-9 shows the PPS1350 in a clustered arrangement against XIPS25. PPS1350 remained limited by lower efficiency, maximum runtime and 46.8% of XIPS-25s I_{sp} but PPS1350 requires 15.55W/mN where the XIPS-25 requires 25.75W/mN. The two-thruster configuration yields greater thrust than the XIPS at a significantly lower power, this indicated that the clustered PPS1350 and various smaller systems may be suitable in cluster arrangements. Finally, it was noted that performance curves in figure-7-8 indicated failure to deorbit within max burn-time occurred at approximately 2100kg.

5.3 Power Source

Energy required (E_m) calculated in table-3-6 excluded the use of batteries to power thrusters. An optimistic average of space-qualified lithium-ion batteries yielded power-densities of approximately 250Wh.kg^{-1} [33]. Given the duration of the missions, the power-supply mass would vary between 70-205 metric-ton.

Solar-arrays were a suitable candidate to generate adequate power. Gallium-arsenide cells (GaAs) are favoured over crystalline silicone in space due to higher efficiencies, and greater resistance to radiation which ensures slower degradation [34]. 3-Junction cell-arrays yield an energy-density of 321Wm^{-2} which meant that the manoeuvre would require 7.8-14.02m^2 of coverage, which would incur additional mass of 90-165kg, if the system was to be an autonomously powered. However, mass-penalties would be avoided if the satellite had enough power available at the end of mission, but must be appropriately oversized to account for redundancies and failures [35].

5.4 Cost Benefit Analysis.

Mass and cost are inextricably linked for space-borne systems. Equation-28 was used to determine ΔV_H for the given altitudes, outputs were then substituted into the Tsiolkovsky Rocket equation [36]. This allowed for the calculation of propellant mass required for an equivalent CP mission, the results were plotted in figure-9.

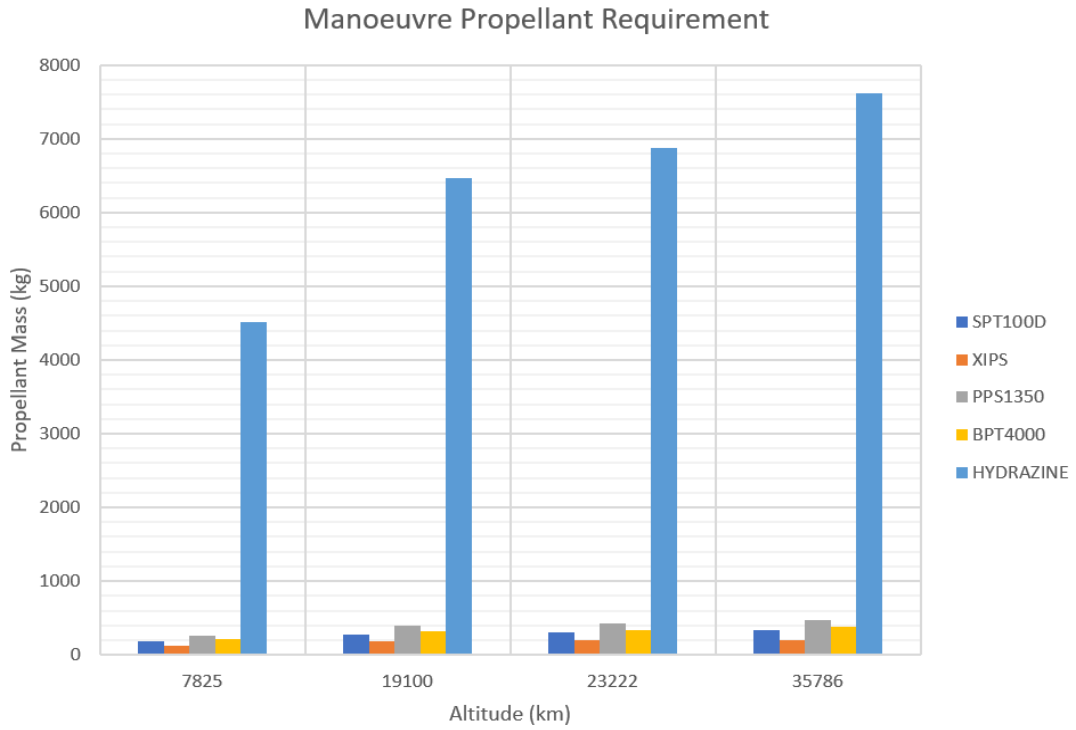

Figure 9 - Propellant mass requirements at tested altitudes for EP & CP.

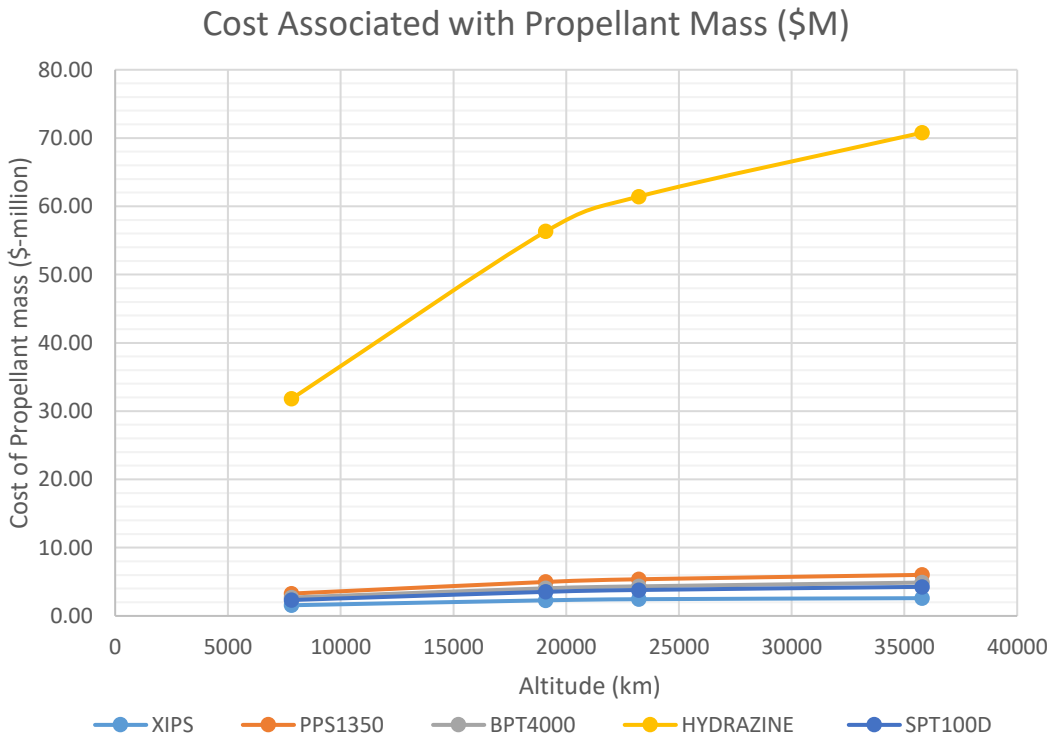

Figure 10 – Costs associated with launching propellant across tested altitudes

It was assumed the 2000kg satellite was launched into a transfer orbit with a Falcon-9 rocket [37]. The $/kg (USD) to launch for a Falcon-9 was calculated as 12,618.55$/kg. Figure-10 displays propellant-cost associated with launch. As expected, the largest propellant-cost was incurred at GEO where EP exceeded $6M, and a hydrazine CP thruster exceeded $70M which made CP unfeasible for use [37]. Therefore, EP incurred an average propellant saving of 94.2%, yielding $30-65M savings across tested altitudes. The analysis relates explicitly to launching extra-propellant, and does not pertain to costing the assosciated technologies.

6.0 Conclusions

The study concluded that EP systems were adequate to manoeuvre a 2000kg MEO and GEO end-of-life satellite to a final orbit of 200km, while conforming with the 25-year mitigation rule, under constant thrust conditions. EP systems would significantly reduce propellant-mass requirements. The propellant-saving could be used to improve payload capacity or reduce propellant costs by at least a factor of ten. BPT4000 and XIPS-25 were the only thrusters capable of performing across all altitudes. Their use would require a trade-off between t_m and propellant savings. While BPT4000 and XIPS-25 were the most appropriate single thrusters, the advantages of clustering smaller thrusters in parallel may yield improved t_m over larger single thrusters. In any case, solar arrays seem the most cost-effective, mission-ready solution in terms of generating power for the manoeuvre. Battery systems were deemed too heavy. Model verification indicated an accuracy greater than 99.99%, but given the timescale of manoeuvres, further-work undertaken would account for all J-parameter perturbations, moons-gravity and solar-radiation pressure to gain a higher degree of accuracy. Furthermore, it would be prudent that further work would include a proposed optimal transfer manoeuvre. Lastly, further work must consider the effectiveness of the ageing control system tasked to react in mitigating further risk of collisions while passing through critical altitudes.

7.0 References

[1] D. Kessler and B. Cour-Palais, “"Collision frequency of artificial satellites: The creation of a debris belt.,” *Journal of Geophysical Research,* vol. 83, no. (A6), p. p.2637., 1978..

[2] Anselmo, P. (ASI), Crowther, T.-S. (BNSC), Alby, Baccini, B. (CNES), A. (DLR), Flury, Jehn and K. (ESA), “"European Code of Conduct for Space Debris Mitigation",” no. Issue 2, p. p.6, 2007.

[3] NASA, “Technical Standard: Process for limiting orbital debris P.41,” National Aeronautics and Space Administation , 25 04 2019. [Online]. Available: file:///C:/Users/gary-/Downloads/nasa-std-8719.14b.pdf. [Accessed 21 03 2020].

[4] J. M. Lafferty, Foundations of vacuum science and technology, New York, N.Y.: J. Wiley and Sons, 1998.

[5] R. G. Jahn, Physics of Electric Propulsion, Mineola, New York: Dover Publications, 2012.

[6] E. Stuhlinger, Ion propulsion for space flight, New York: McGraw-Hill, 1964.

[7] George P Sutton and O. Biblarz, “Electric Propulsion,” in *Rocket Propulsion Elements*, Hoboken, New Jersey, Wiley Interscience, 2010, pp. p.622-658.

[8] E. P. Division, “Satellite Power Systems,” Technology Programmes in Space, [Online]. Available: http://www.esa.int/esapub/br/br202/br202.pdf. [Accessed 24 02 2020].

[9] NASA, “The Prius of Space,” NASA Jet Propulsion Laboratory, September 2007. [Online]. Available: https://www.jpl.nasa.gov/news/?feature=1468. [Accessed 26 02 2020].

[10] W. B. Machine, “Asteroid explorer Hayabusa-mounted ion engin,” Internet Archive , 2015. [Online]. Available: https://web.archive.org/web/20060819093452/http://www.ep.isas.ac.jp/muses-c/. [Accessed 03 03 2020].

[11] J. S. Sovey, V. K. Rawlin and M. J. Patterson, “Ion Propulsion Development project in US. Space Electric Rocket Test I to Deep

Space 1," *Journal of Propulsion and Space ,* vol. Volume 17, no. 3, pp. P.517-526, 2001.

[12] R. A. C. Schonenberg and H. F. R. Schoyer, "Solid Propulsion De-orbiting and Re-orbiting," *NASA Astrophysics Data System ,* p. p.67, 03 01 2009.

[13] MIT, "Analytical Approximations for Low Thrust Maneuvers," *MIT Openware,* vol. https://ocw.mit.edu/index.htm, p. p.3, 2015.

[14] T. Oliphant and P. Pearu, "ntegration and ODEs (scipy.integrate)," SciPy, 2001. [Online]. Available: https://docs.scipy.org/doc/scipy/reference/integrate.html. [Accessed 20 10 2020].

[15] T. Oliphant, "NumPy v1.19.dev0 Manual," NumPy, 2006. [Online]. Available: https://numpy.org/. [Accessed 1 09 2020].

[16] R. Battin, An Introduction to the Mathematics and Methods of Astrodynamics, NY: AIAA, 1999.

[17] F. A. Tewari, Atmospheric and Spaceflight Dynamics, Modelling and Simulations with MATLAB and SIMULINK, New York: Springer, 2007.

[18] J. C. Butcher, "Adams Method," in *Numerical Methods for Ordinary Differential Equations*, Hoboken, Ney Jersey, Wiley, 2003, pp. p105-121.

[19] P. J. Montenbruck and G. Eberhand, "Keplarian Orbital Elements," in *Satellite Orbits: Models, Methods, Applications.*, New York, Springer, Heidelberg, 2005, p. p28.

[20] R. Schwarz, "Cartesian State Vectors > Keplerian Orbit Elements (Memorandum #2)," 2017. [Online]. Available: rene-schwarz.com. [Accessed 13 1 2020].

[21] H. Curtis, "Section 4.7," in *Orbital Mechanics for Engineering Students*, London, Heinemann, 2005, pp. p.177-181.

[22] H. J. Anton , C. De Ruite and J. R. Forbes, Spacecraft dynamics and control : an introduction, Hoboken, Ney York: Wiley, 2012.

[23] National Aeronautics and Space Administration,, "The Drag Equation - Glen Research Centre," Glen Research Centre, 2012. [Online].

Available: https://www.grc.nasa.gov/www/k-12/airplane/drageq.html. [Accessed 17 01 2020].

[24] D. M. Prieto, B. P. Graziano and P. C. E. Roberts, “Spacecraft Drag Modelling,” *Progress in Aerospace Sciences,* pp. p 2-3, 2016.

[25] National Aeroautics and Space Administration, “US Standard Atmosphere 1976,” NASA, 10 1976. [Online]. Available: https://ntrs.nasa.gov/archive/nasa/casi.ntrs.nasa.gov/19770009539.pdf . [Accessed 05 02 2020].

[26] A. M. Society, “Glossary of Meteorlogy: Scale Height,” American Meteorological Society , 2012. [Online]. Available: http://glossary.ametsoc.org/wiki/Scale_height. [Accessed 12 02 2020].

[27] S.-H. Chen, “ATM60 - Coriolis Effect,” University of California Davis, 2013.

[28] R. G. Jahn and E. Y. Choueiri, “Electric Propulsion Encyclopedia,” *Encyclopedia of Physical Science and Technology,* vol. Volume 5, no. Third edition, pp. p.125-137, 2002.

[29] T. S. Kelso, “Active elements,” Celestrak, 01 03 2020. [Online]. Available: https://www.celestrak.com/Norad/elements/active.txt. [Accessed 02 03 2020].

[30] F. Covello, “Application of electrical propulsion for an active debris removal system: a system engineering approach.,” *Advances in Space Research (COSPAR),* vol. 50, no. 918-931, pp. P.3-5, 2012.

[31] A. Ionel, “Performance evaluation of propulsion systems as LEO deorbiting devices,” *INCAS - National Institute for Aerospace Research,* vol. 9, no. 3, pp. p.55-69, 2017.

[32] A. Gaudel, C. Hourtolle, J. F. Goester and M. Ottavianni, “De-orbit stratagies with Low Thrust Propulsion,” in *Mission Architecture For Active Space Debris Removal Using The Example of SL-8 Rocket Bodies*, Hoboken, Springer, 2015, pp. P.55-59.

[33] S. Luong, “What is a lithium-ion battery and how does it work?,” Clean Energy Institude - University of Washington, 2020. [Online]. Available: https://www.cei.washington.edu/education/science-of-solar/battery-technology/. [Accessed 2020 03 09].

[34] S. Bailey and R. Ryne, “Operation of Solar Cells in a Space Environment,” in *Practical Handbook of Photovoltaics*, Amsterdam, Elseveir, 2012, pp. p.863-870.

[35] M. A. V, “GaAs and highly efficient space cells,” in *Practical Handbook of Photovoltaics: Fundamentals and Applications*, Amsterdam, Elseveir, 2012, pp. p.319-413.

[36] D. Pettit, “The Tyranny of the Rocket Equation,” NASA, 05 01 2012. [Online]. Available: https://www.nasa.gov/mission_pages/station/expeditions/expedition30/tryanny.html. [Accessed 2020 02 25].

[37] SpaceX, “Capabillities & Services,” SpaceX, [Online]. Available: https://www.spacex.com/about/capabilities. [Accessed 15 03 2020].

[38] D. M. Goebel, “Ion & Hall Thrusters,” in *Fundamentals of electric propulsion*, Hoboken, NJ, Wiley, 2008.

8.0 Appendices

8.1 Source-code Hyperlink

https://github.com/Gary-stewart1992/GS-ME409

(The source code far exceeds the two-page appendix limit, so could not be placed within this work)

8.2 Satellite Details

Devised Satellite Details			
Satellite Name	**Dry Mass (kg)**	**Satellite Cross-section (m^2)**	**Coefficient of Drag**
Sat-1	2000	5.60E-06	2.2

8.3 Auxiliary Orbital Element plots

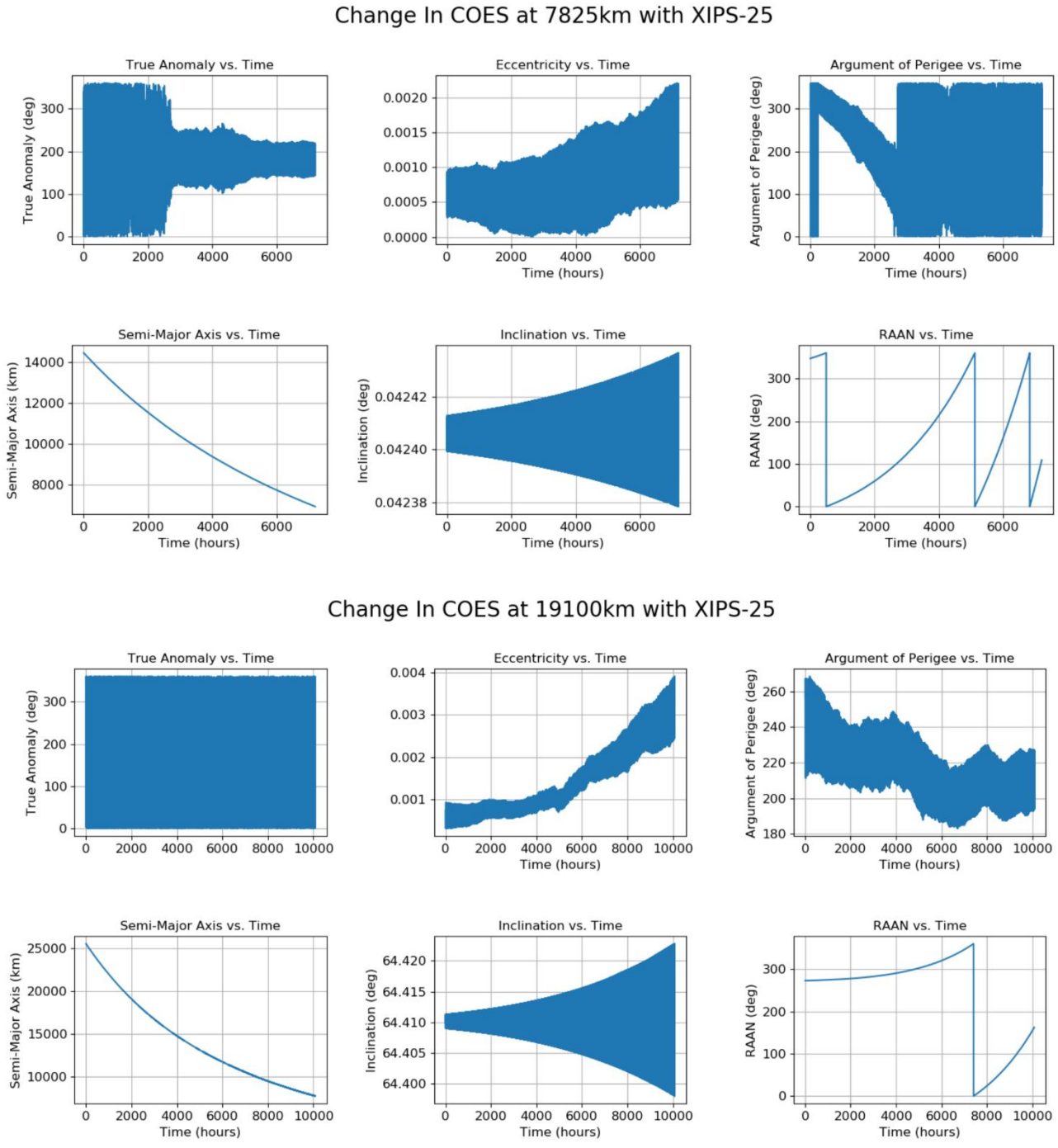

Change In COES at 23222km with BPT4000

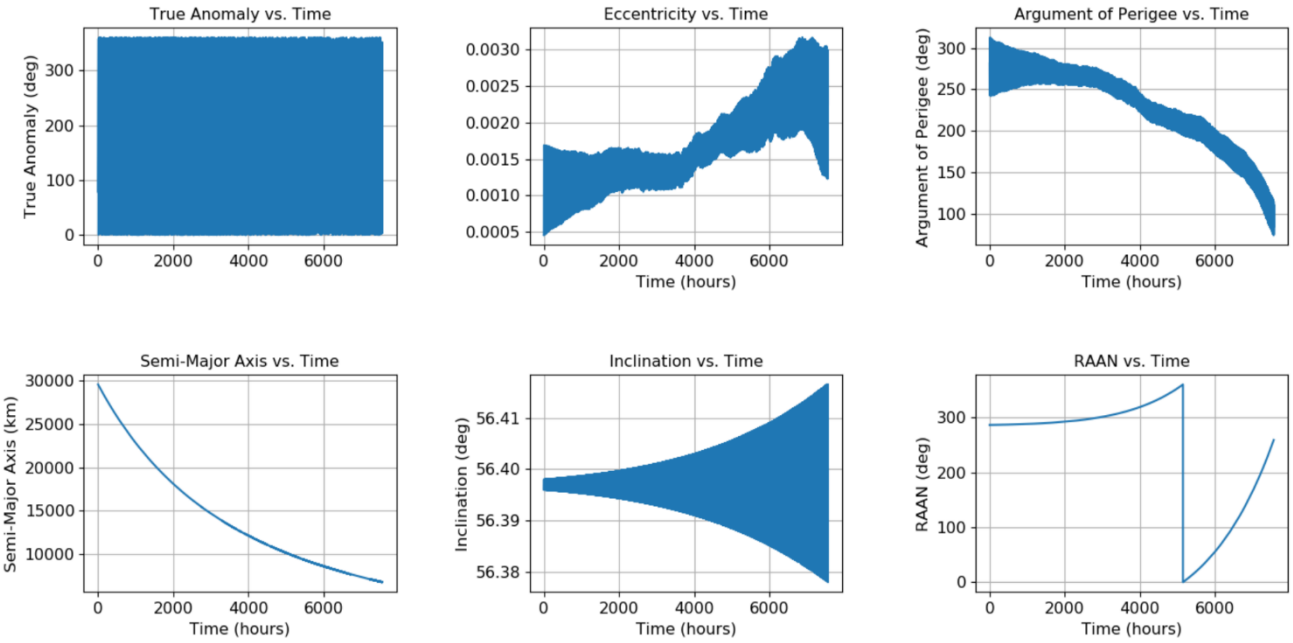

Change In COES at 35786km with BPT4000